Molecular dynamics computations of brine-CO_2 interfacial tensions and brine-CO_2-quartz contact angles and their effects on structural and residual trapping mechanisms in carbon geo-sequestration

S. Iglauer[1*], M.S. Mathew[2], F. Bresme[2,3*]

[1]Curtin University, Department of Petroleum Engineering, 26 Dick Perry Avenue, 6151 Kensington, Australia; phone: +61 8 9266 7703

[2]Department of Chemistry, Imperial College London, SW7 2AZ London, United Kingdom; phone: +44 0207 594 5886

[3]Department of Chemistry, Norwegian University of Science and Technology, NO-7491, Trondheim, Norway.

[*]corresponding authors

Abstract

In the context of carbon geo-sequestration projects, brine-CO_2 interfacial tension γ and brine-CO_2-rock surface water contact angles θ directly impact structural and residual trapping capacities. While γ is fairly well understood there is still large uncertainty associated with θ. We present here an investigation of γ and θ using a molecular approach based on molecular dynamics computer simulations. We consider a system consisting of CO_2/water/NaCl and an α-quartz surface, covering a brine salinity range between 0 and 4 molal. The simulation models accurately reproduce the dependence of γ on pressure below the CO_2 saturation pressure at 300 K, and over predict γ by ~20% at higher pressures. In addition, in agreement with experimental observations, the simulations predict that γ increases slightly with temperature or salinity. We also demonstrate that for non-hydroxylated quartz surfaces, θ strongly increases with pressure at subcritical and supercritical conditions. An increase in temperature significantly reduces the contact angle, especially at low-intermediate pressures (1-10 MPa), this effect is mitigated at higher pressures, 20 MPa. We also found that θ only weakly depends on salinity for the systems investigated in this work.

Keywords: molecular dynamics, CO_2 contact angles, carbon geo-sequestration, structural trapping, residual trapping, CO_2-brine interfacial tension

1. Introduction

The spreading behaviour of two immiscible or partially miscible fluids on a solid surface is a fundamental phenomenon of great relevance in interfacial science, with wide technological and scientific implications, ranging from fields so different as zoology [1] to civil engineering [2] and semiconductor manufacturing [3]. In this work we discuss the spreading behaviour of fluids on mineral surfaces relevant to carbon geo-sequestration (CCS), which has been identified as a key element to mitigate anthropogenic carbon dioxide (CO_2) emissions to the atmosphere [4]. In CCS, CO_2 is commonly injected at 800 m depth or deeper so that the CO_2 is in a supercritical (sc) state thereby increasing storage capacity. Target formations are depleted oil or gas reservoirs or deep saline aquifers. Although the CO_2 is in a sc phase it is lighter than the resident formation brine and migrates upwards due to buoyancy forces. However there are four trapping mechanisms, which keep the CO_2 in the subsurface: a) structural trapping [5], b) residual trapping [6-8], c) dissolution trapping [9,10] and d) mineral trapping [11]. Each storage mechanism is active on different time scales and the two most important storage mechanisms during the first several hundreds of years of a storage project are *structural* and *residual* trapping. The present article discusses a situation that is relevant to these two mechanisms.

The primary storage mechanism is structural trapping, where CO_2 is trapped beneath a seal layer, which has a very low permeability. The column height h (i.e. volume) of CO_2 stored safely beneath such a caprock is directly proportional to the cosine of the contact angle between water, $scCO_2$ and the caprock [12] (measured through the water):

$$h = \frac{p_{c,e}}{\Delta\rho g} = \frac{\gamma \cos\theta}{R\Delta\rho g} \qquad (1)$$

Where $p_{c,e}$ is the capillary entry pressure ($p_{c,e} = \gamma \cos\theta / R$), γ is the CO_2-brine interfacial tension, R is the effective pore radius, g is the acceleration due to gravity, $\Delta\rho$ is the CO_2-brine density difference, and θ is the water-CO_2-mineral surface contact angle. CO_2 can break through the caprock if stored above the CO_2 break-through pressure $p_{c,e}$ and there are currently no efficient technologies which can counter such caprock leakage.

The secondary storage mechanism, residual trapping, is especially relevant in cases where there is no caprock or the existence of the caprock is unproven. In addition, residual trapping reduces lateral and vertical migration of CO_2 thereby reducing leakage risk [13]. In residual or capillary trapping the $scCO_2$ is immobilized by capillary forces [4,8] in the micro-scale pore network of the rock. However, residual trapping capacity is a function of the exact wetting behaviour in the rock, i.e., the contact angle in each pore (see Figure 2 in Ref. [14]), the pore morphology of the rock, and the CO_2-brine interfacial tension. Generally, low values of γ are detrimental for structural (equation 1) and residual trapping [15], and more CO_2 is trapped when the water contact angle θ is low [14,16]. Furthermore, residual trapping is a function of initial CO_2 saturation and rock porosity [7,8,17-22] In this context we defined the capillary trapping capacity (C_{trap}) of porous rock, which is the product of residual CO_2

saturation and porosity [22]. C_{trap} ranks rocks according to their quality as residual trapping CO_2 storage medium.

It stems from the discussion above that an accurate knowledge of contact angles and interfacial tensions is vital to predict potential CO_2 leakage, estimate residual and structural trapping capacities and thereby improve risk and capacity assessments and containment security. While γ is fairly well understood, e.g. see references [23-28], θ has received less attention. Moreover, the experimental results available for θ in the literature have significant uncertainties, to the extent that the data obtained so far are somewhat inconclusive, e.g., see the recent discussion in the *International Journal of Greenhouse Gas Control* [29-31].

However, several researchers have measured θ on various substrates as a function of pressure, temperature and salinity conditions [27,29,32-35]. These investigations included water-wet surfaces: quartz, mica, calcite, biotite, orthoclase, labradorite [27,29,32,35], but also mixed-wet surfaces: silica coated with Maracaibo Lake crude oil [27] and a carbonate from the Weyburn oilfield [34], and oil-wet surfaces: polytetrafluoroethylene [27] and a partially methylated glass surface [33].

One important conclusion that follows from the analysis of the above experiments is that mixed-wet and oil-wet surfaces can be CO_2-wet, i.e. $\theta > 90°$ was measured. A CO_2-wet surface, however, has serious consequences in terms of structural trapping: CO_2 will spontaneously imbibe into the caprock and, flow upwards due to buoyancy forces – albeit slowly because of the low absolute permeability of the seal rock. In addition, as mentioned above, residual trapping will be significantly reduced [14]. It is therefore important to identify CO_2-wet conditions so that worst-case scenarios, i.e. CO_2 leakage to the surface, can be avoided.

In terms of water-wet surfaces, some datasets were published which reached inconsistent conclusions. While Chiquet et al. [32] measured an increase in θ with increasing pressure for quartz (an increase from approximately $\theta = 22°$ to $\theta = 38°$ for a pressure increase from 1 MPa to 9 MPa, 0.2 M salt concentration and 308K [36]), Espinoza and Santamarina [27] measured an approximately constant θ ($\approx 40°$) with increasing pressure (also for a 0.2 M salt solution, 1-10 MPa pressure interval, but slightly lower temperature, 298K). Bikkina [29] also measured a constant θ with increasing pressure, and he found that the number of CO_2 exposure cycles had a very strong influence on θ. He measured a θ between 25-30° for the first CO_2 exposure cycle, but a strongly increased θ, between 65-70°, for a second CO_2 exposure cycle. Bikkina [29] used deionized water, and tested the pressure range 3-20 MPa at a temperature of 298K. Bikkina explained the cycle-effect with H_2O-dehydration from the water-wet surface by $scCO_2$, although this explanation is currently debated [30,31]. Mills et al. [35] measured a θ between 27-32° for carbonated brine at 12.9 MPa, 313.15K, in a 35000 ppm salt solution. In addition, Mills et al. [35] measured a drop in advancing θ with an increase in pressure (θ was 38-40° at sub-critical CO_2 conditions, p = 5.8 MPa, T = 313.15K and θ was 27-38° for $scCO_2$ conditions, p = 13 MPa, T = 313.15K for non-carbonated, plain, brine; i.e. a non-equilibrated fluid system; note that fluid equilibration processes may influence θ).

Furthermore, Chiquet et al. [32] measured only a small influence of salinity on θ, he found that θ decreased slightly with salinity (approximately by 5° for a 1M salt solution – compared with a 0.2 M solution); however, Espinoza and Santamarina [27] found a significant difference between deionized water and salt solutions, they measured a 20° increase in θ if salt was added to the system (200 g NaCl/kg water). It is possible that small amounts of salt significantly change θ, and this is one question, which we will discuss in more detail later in the manuscript. For calcite similar conclusions were reached.

It is worth noting that only Chiquet et al. [32] and Mills et al. [35] have performed the measurements at representative reservoir conditions, namely at high pressure and elevated temperature conditions using brine (deionized water is not found in geologic reservoirs). Typical storage conditions in a deep saline aquifer are 10 MPa fluid pressure, 323K and 2 M brine [7]. In our opinion the large uncertainty currently associated with θ may be caused by subtle differences in temperature (measurements above or below 304.5K, which is the critical temperature of CO_2), as the CO_2 is then either supercritical or subcritical. However, our main belief is that – although we think that supercritical and subcritical conditions play a significant role – the θ measurements are notoriously difficult and even minute contaminations could have a major impact.

Chalbaud et al. [25] conducted pore scale wettability studies for glass micromodels with different hydrophilicities: water-wet, intermediate-wet and oil-wet. They tested CO_2 wetting for gaseous CO_2 (p = 6 MPa, T = 292-298K), liquid CO_2 (p = 10 MPa, T = 296-298K), and scCO_2 (p = 10-10.5 MPa, T = 333K), and they observed several effects: 1. In case of the water-wet surface, CO_2 was non-wetting for all thermo-physical conditions, although no water surface films were identified at high pressures. 2. At high pressures for the intermediate and oil-wet surfaces, CO_2 was identified as the wetting phase. 3. CO_2 wettability was stronger at lower temperatures.

Moreover, in a capillary pressure experiment, Plug and Bruining [37] found at a pressure of 8.5 MPa and a temperature of 313 K that clean quartz sand can be CO_2-wet during water flooding (above a water saturation of 0.5).

In order to shed more light into mineral-CO_2 interactions and to more fundamentally understand the relationship between θ and true reservoir conditions, we have conducted a computational molecular dynamics (MD) study. This approach can a) provide additional data, without the experimental uncertainties associated with the topology and chemical composition of the surfaces, hence increasing confidence and reducing uncertainty, b) provide a platform with which results can be rapidly and economically generated, and c) provide detailed results at a molecular level, which significantly broadens our fundamental understanding of CO_2/water/mineral surface interactions. To the best of our knowledge, the first MD simulations of the wetting behavior at CO_2/water/solid interfaces were performed by Liu et al. [38]. Liu et al. concluded that θ on their hydrophilic surface increases with CO_2 fluid density. These authors did not consider the influence of salinity or temperature on the contact angle, which we will discuss here.

2. Computational Methods

We have performed simulations for CO_2-water interfaces and water droplets adsorbed on a quartz surface as a function of temperature, salinity and CO_2 pressure. We used the TIP4P/2005 potential model for water [39] and the EPM2 model for CO_2 [40]. The intermolecular interactions were modelled through Lennard-Jones (LJ) and Coulomb potentials. The TIP4P/2005 model quantitatively reproduces the surface tension of the corresponding liquid-vapour interface [41], hence it represents a good starting point to investigate the properties of the H_2O-CO_2 interface. Indeed these two models have been used in previous simulation studies, showing good agreement with experiments at elevated temperatures and high pressures (CO_2 in a supercritical state) [42,43].

As a starting point for future systematic investigations of contact angles on quartz surfaces we consider here an α-quartz surface with a Si-O-Si bridge surface structure (see Figure 1). Previous studies using density functional computations have shown that water physisorbs without dissociating on the fully coordinated Si-O-Si bridged surface [44]. However, in under-coordinated surfaces the formation of silanol groups is energetically favoured. We investigate in this work the fully coordinated surface, and therefore no silanol groups are included.

A periodically repeating super cell was created from an orthorhombic unit cell to model the α-quartz slab. The transformation from the hexagonal unit cells to the orthorrombic one was performed as discussed in ref. [45]. Subsequently the unit cell was replicated to create a crystal that was equilibrated at 0.1 MPa pressure, and used later to create the α-quartz slabs employed in the simulations of the systems containing CO_2 and water.

The force field parameters used in this work to model the quartz surfaces are listed in Table 1. The interatomic potential used in the quartz simulation is [46]:

$$u_{ij}(r) = \frac{q_i q_j e^2}{4\pi\varepsilon_0 r} + A_{ij}\exp[-b_{ij} r] - \frac{C_{ij}}{r^6} \qquad (2)$$

where, u_{ij} represents the interaction between atoms *i* and *j* at distance r , q_i is the point charge on atom *i,* and the constants A_{ij}, C_{ij}, and b_{ij}, are taken from reference [46].

Table 1
Force field parameters for the SiO_2 surface (Ref. [46]). Si-Si interactions are modelled with the coulombic potential only, i.e., A_{SiSi}=0 and C_{SiSi}=0.

Interaction	A_{ij} /[kJ/mol]	b_{ij} /[Å^{-1}]	C_{ij} [(kJ/mol) Å^6]	q_i/e
O-O	1.34015×10^5	2.76	1.6887×10^4	q_O=-1.2
Si-O	1.7373×10^6	4.873	1.2886×10^4	q_{Si}=2.4

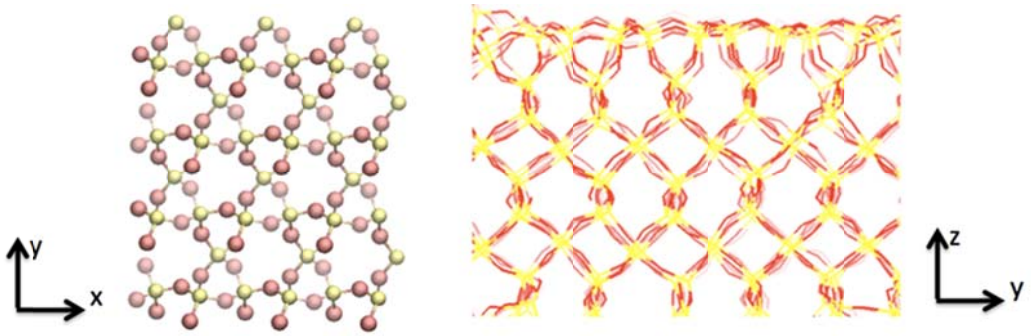

Figure 1. (Left) 3x2x2 supercell of an α-quartz crystal. (Right) Snapshot of an α-quartz surface after relaxation over 100 ps, showing the Si-O-Si bridged structure on the top surface (Red spheres/lines-oxygen, Yellow spheres/lines-Silicon).

The dispersion interactions for water, CO_2 and the ions were computed using the Lennard-Jones model,

$$u_{ij}(r) = 4\,\varepsilon_{ij}\left[\left(\frac{\sigma_{ij}}{r}\right)^{12} - \left(\frac{\sigma_{ij}}{r}\right)^{6}\right], \qquad (3)$$

where ε_{ij} is the interaction strength between atoms i and j separated by a distance r, and σ_{ij} is the effective diameter of these atoms (see Table 2). To derive the cross interactions between atoms belonging to different molecules we employed the Lorentz Berthelot mixing rules, $\sigma_{ij} = (\sigma_{ii} + \sigma_{jj})/2$, $\varepsilon_{ij} = \sqrt{\varepsilon_{ii}\,\varepsilon_{jj}}$, where σ_{ii} and ε_{ii} are the diameter and interaction strength, respectively, for atom i. The parameters to model sodium chloride have been optimized recently in Ref. [47] to model aqueous solutions at low and high concentrations, including saturation conditions. Hence in this paper we employ the parameters derived in that work.

The cut-off for the Van der Waals (vdW) interactions was set to 17 Å to ensure the long-range contribution to the interfacial tension is negligible. Long-range Coulombic interactions were computed using the Ewald summation method [48]. All simulations were run using periodic boundary conditions except in the simulations of the contact angles, where a soft repulsive potential was set in the direction normal to the quartz surface in order to confine the CO_2 molecules to the upper part of the simulation box. The soft repulsive force was harmonic, $f_{rep} = -k(z - z_0)$, where k = 1 kJ/mol is the force constant, and z_0 determines the location of the repulsive potential, which was set far from the SiO_2 surface, 55 Å, to ensure the perturbation of the CO_2 density by the repulsive confining force does not affect the contact angle estimates at the quartz surface. The simulations were run for 5×10^4 equilibration steps and $0.5\text{-}1\times10^6$ production steps, with a time step of 0.002 pico-seconds. All the simulations were performed in parallel using the code DL_POLY 2.19 [49].

Table 2
Lennard-Jones parameters employed in the computer simulations performed in this work. The water model parameters correspond to the TIP4P/2005 model [39], the CO_2 parameters to the EPM2 model [40], SiO_2 and NaCl parameters to the models described in [46,47].

Site	ε/ (kJ/mol)	σ/Å	q/e
O (water)	0.77502	3.1589	0
M (water)	0	0	-1.1128
H (water)	0	0	0.5564
C (CO_2)	0.23391	2.757	0.6512
O (CO_2)	0.66947	3.033	-0.3256
Si	0.5335	3.795	2.4
O (quartz)	0.6487	3.154	-1.2
Na^+	0.196	2.45	+1
Cl^-	0.628	4.1	-1

3. Results and discussion

3.1 CO_2-water interfacial tensions

The interfacial tension γ of the CO_2-water interface has been previously computed using the EPM2-TIP4P/2005 models, which are also employed in this work [42,43]. These studies focused on high temperature and pressure (383 K and 4-45 MPa). We consider here subcritical and supercritical states and analyze the influence of pressure on γ. Hence we have performed canonical simulations (N,V,T) in a simulation box with dimensions 56.61 × 56.61 × 105.5 $Å^3$ in the x, y and z directions to cover the thermodynamic states of interest to us. This simulation set up results in a cross sectional area that is large enough to minimize the periodic error effects discussed by González-Melchor et al. [50]. The simulations were run at 300 K, 343 K and 350 K, and the CO_2 pressure was modified by varying the number of CO_2 molecules in the simulation box (between 10 and 2048 CO_2 molecules). A total of 5832 water molecules were used for each simulation. We ignore here the presence of protons, HCO_3^- and CO_3^{2-} anions, which result from the dissociation of H_2CO_3 in the aqueous phase [9]. As noted in reference [51], for typical experimental conditions (Schaef and McGrail [52] measured a pH value between 3-4 for storage conditions) the amount of ions per water molecule is very low, ~10^{-3}, hence we did not include them in the presented computations. We expect this will cause a very small effect on the computed interfacial tensions and contact angles [53].

The CO_2 pressure was computed using the pressure component normal to the CO_2-water interface. No long-range corrections for the pressure were included in these computations. γ was then calculated from the microscopic expression of the pressure tensor,

$$\gamma = \frac{L_z}{2}\left[P_{zz} - \frac{1}{2}(P_{xx} + P_{yy}) \right] \quad (6)$$

where $P_{\alpha\beta}$ are the pressure tensor components with α and β being the cartesian coordinates (x, y, z), and L_z the box length in the direction normal to the interface. The pressure components were obtained from the virial equation,

$$P_{\alpha\beta}V = \sum_{i=1}^{N} m_i \, \mathbf{v}_{i,\alpha}\mathbf{v}_{i,\beta} + \sum_{i=1}^{N-1}\sum_{j>i}^{N} \mathbf{r}_{ij,\alpha} \, \mathbf{f}_{ij,\beta} \, , \qquad (7)$$

where $\mathbf{v}_{i,\alpha}$ is the velocity of atom i in direction α, $\mathbf{r}_{ij} = \mathbf{r}_i - \mathbf{r}_j$, $\mathbf{f}_{ij}$ is the force exerted on atom i by atom j, and V is the volume of the simulation box.

Our simulated isotherms for subcritical and supercritical states (see Figure 2) are in good agreement with experimental data [54,60], and also agree well with previous simulations [56] at 300 K, in the low-pressure range. Nonetheless some deviations are noticeable when approaching the vapour-liquid transition. We also find some deviations at higher pressures. One possible reason for this difference could be the treatment of the cut-off in previous work. A shorter cut-off would result in a slight reduction in the critical temperature predicted by the EPM2 model using Molecular Dynamics simulations as compared with the Monte Carlo simulations using the same cut-off and long-range corrections. The longer cut-off used here, 17 Å, should provide a better reproduction of the original Monte Carlo results which correspond to the full potential.

3.1.1 CO_2-water interfacial tensions as a function of pressure

Figure 3 shows our results for the dependence of the interfacial tension, γ, on CO_2 pressure. γ drops rapidly until it reaches a pressure of ~6.7 MPa and then stays approximately constant. The change in the interfacial tension coincides with the saturation pressure of CO_2 at 300 K, which is well reproduced by the EPM2 model (see Figure 2). Our simulated interfacial tensions closely follow the available experimental data at pressures below the vapour-liquid transition at 300 K (p_{CO2} = 6.7 MPa [57]), this represents an improvement over previous simulation data, which used in most cases the SPC/E potential to model the water phase [56]. It is however well known that the SPC/E model under predicts the surface tension of water at ambient temperature by ~10% [41,58], hence it is inaccurate at low CO_2 pressures, where the water surface dominates the interfacial free energy. At high CO_2 pressures, above 6.7 MPa, the models used in this work over predict the experimental interfacial tension by ~20%. Interestingly, the computed interfacial tensions agree with data previously obtained with the SPC/E model at slightly higher temperatures 323 K (see Figure 3). Experiments have shown that γ increases with increasing temperature. This dependence is not captured by all simulation models; for example, da Rocha et al. [51] reported a reduction in γ when using the SPC/E model at high pressures, 20 MPa. Overall, the accuracy of the water force-field is essential to obtain good estimates of the CO_2-water interfacial tension at low-intermediate pressures and subcritical temperatures, whereas it seems to play a less important role in determining the interfacial tension at high CO_2 pressures.

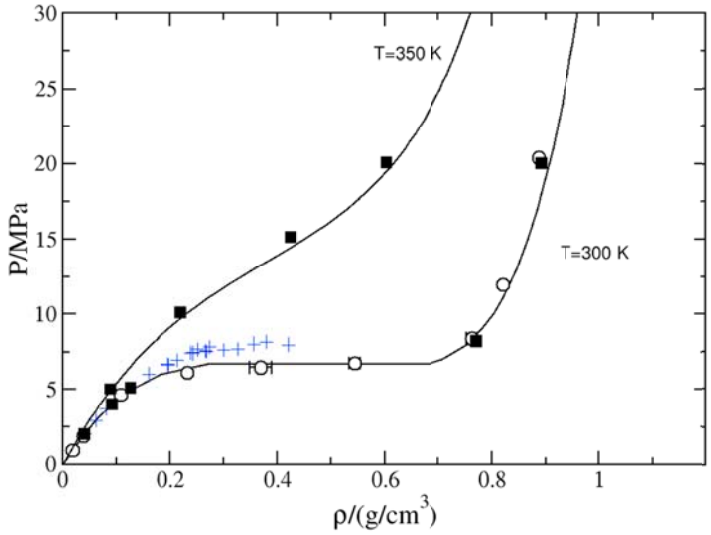

Figure 2. Pressure-density CO_2 isotherms at 300 K and 350 K. Full line (ref. [57]). Symbols represent simulation data obtained using the EPM2 model. Open circles: this work, obtained from simulations with the explicit CO_2-water interface; squares: this work using NPT simulations of pure CO_2 using a 12 Å cut-off and including long range corrections; crosses – reference [56].

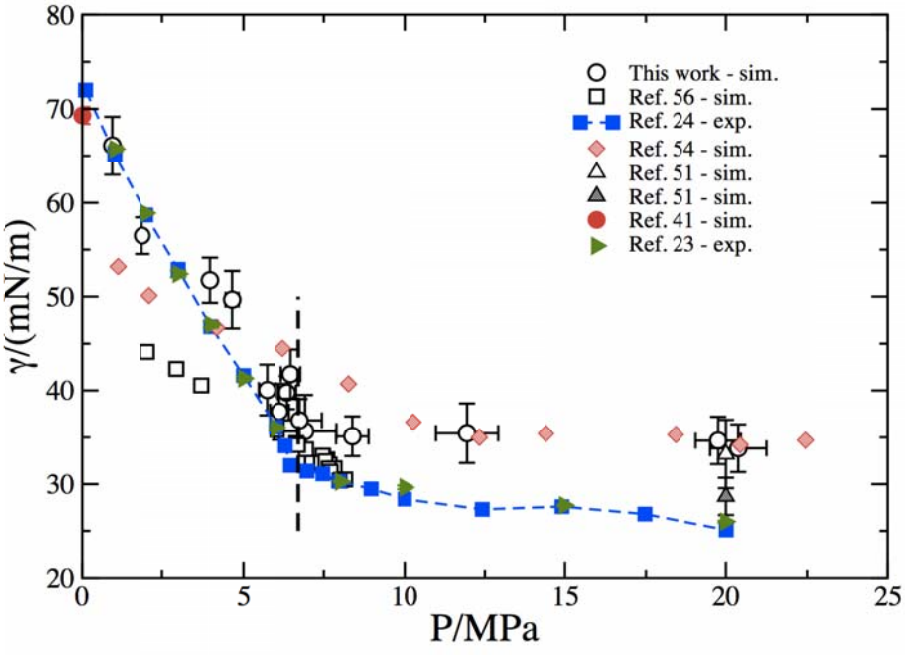

Figure 3. Interfacial tension of the water-CO_2 interface as a function of pressure for various experimental and simulation results. Filled squares – experiments at 298.3 K from reference [24]; right triangles – experiments at 297.9 K from reference [23]; open circles – simulations performed in this work at 300 K; filled circle – interfacial

tension of the TIP4P/2005 water interface (reference [41]); Triangles up – simulations at 318 K (open) and 338.15 K (filled) using the SPC/E model (from reference [51]); diamonds – simulations using the SPC/E model at 323 K (from reference [54]); open squares – simulations using the SPC/E model at 300 K (from reference [56]). The vertical dashed line indicates the saturation pressure of CO_2 at 300 K (reference [57]).

3.1.2 CO_2-water interfacial tensions as a function of temperature

As pointed out above, previous investigations using the TIP4P and EPM2 models at elevated temperatures showed reasonable agreement with experimental interfacial tension data. Again, the simulation results overestimate the interfacial tension by about 10-20%. We have performed additional simulations at 343 K and 350 K, and different pressures (cp. Table 3). Our data show an increase of γ with temperature at intermediate pressures. We also find that the difference between the interfacial tensions at low and high temperatures increases as the pressure decreases. The simulated temperature and pressure dependence agrees with the experimental results [23]. At high pressures however, ~20 MPa, we do not find significant differences between the data at 300 K and 350 K. In fact the interfacial tensions are identical within the statistical accuracy of the computations. This might indicate that at higher pressures longer simulations will in general be required to observe clear trends, and may explain why a reduction in γ with increasing temperature was observed in previous simulation work [51]. The significant difference between computed and experimental γ at higher pressures (e.g. compare data for T = 343 K in Table 3) highlights a deficiency of the TIP4P/2005 water and EPM2 CO_2 models. One possible reason for these deviations could be that in using the Lorentz-Berthelot combining rules we are missing non-additive contributions between the CO_2 and water, which would be significant at high pressures, i.e. high CO_2 densities.

Table 3
Interfacial tensions of the CO_2-water interface obtained from computer simulations, as a function of temperature, pressure and salt concentration. Experimental data (Exp.) taken from reference [23].

T/K	P/MPa	Salt concentration/molal	γ/(mN/m)
350	6.4±0.1	0	45.8±0.5
350	11.7±0.3	0	39.4±0.7
350	16.3±0.4	0	35.3±0.8
350	19.5±0.5	0	33.3±0.9

T/K	P/MPa	Salt concentration/molal	γ/(mN/m)
343.3 (Exp.)	12.05	0	32.75±0.19
343	12.3±0.5	0	38.5±0.9
343.3 (Exp.)	20.20	0	28.36±0.12
343	19.3±0.6	0	33.9±1.5

T/K	P/MPa	Salt concentration/molal	γ/(mN/m)
300	0.92±0.1	0	66.09±3.1
300	1.9±0.1	0	56.5±2.0
300	4.7±0.2	0	49.7±3.1
300	6.1±0.3	0	37.7±3

300	6.8±0.7	0	36.8±2.3
300	8.4±0.5	0	35.1±2
300	11.9±1	0	35.4±3.1
300	20.4±0.9	0	33.8±2.5

T/K	P/MPa	Salt concentration/molal	γ/(mN/m)
300	19.1±0.6	0.17	35.4±1.1
300	16.1±0.5	1.0	36.1±1.
300	14.0±0.3	2.1	38.05±1
300	12.8±0.5	3.4	43.8±1.8

3.1.3 CO_2-water interfacial tensions as a function of salinity

In order to investigate the influence of salt concentration on the CO_2-water interfacial tension we constructed a CO_2-brine model by substituting water molecules with NaCl ion pairs, so as to achieve a desired salt concentration. Of course formation water, i.e., the water in an oil reservoir or aquifer, is saline and it can reach very high salinities (for instance total dissolved salt concentrations of up to 338 g/L were measured in the Eocene Shahejie Formations in the Dongying Depression [59]). Despite this fact the influence of salt on γ has not been considered systematically in previous computer simulation studies. In a very recent work the effect of 2.7 M $CaCl_2$ on γ has been investigated, showing that the addition of salt results in an increase of the interfacial tension [55].

We have investigated NaCl solutions with molalities ranging from 0-3.5 m, a range that is relevant to CCS. Addition of salt results in a contraction of the water solution, i.e., a change in the osmotic pressure, which is reflected in the pressure normal to the interface. Comparison of the interfacial tension at a particular pressure and molality with the zero salt case clearly shows that addition of salt increases the interfacial tension. For the higher salt concentrations investigated here, the interfacial tension increase is significant, approximately 20%. Chalbaud et. al. [25] have performed an extensive experimental analysis of the dependence of γ on salt concentration. For T=300 K they concluded that the increase in γ with molality is approximately linear for pressures higher than the saturation pressure. This conclusion is based on considering all their experimental data, assuming that the increase in the interfacial tension is independent of pressure for pressures above the CO_2 saturation pressure. Under these conditions they report a linear increase in γ with molality, $\Delta\gamma(m)=\gamma(m)-\gamma(0)=1.43m$ (mN/m) where m is the molality of the solution. This equation is valid for the interval investigated in those experiments, (0.085, 2.75) *m*. We have used this equation to estimate the increase in γ for our molalities using the interfacial tension data in Table 3. The increase in interfacial tension was obtained by subtracting the interfacial tensions of the CO_2-brine and the CO_2-water interfaces, at the CO_2 pressure corresponding to the CO_2-brine interface (see Table 3). The interfacial tensions of the CO_2-water interface at the corresponding pressure were estimated by interpolation of the simulation data reported in Figure 2. We have focused on higher salt concentrations, > 1M, as the simulation approach provides more accurate estimates in this interval. The consistency between the simulated results and the experimental estimates for the higher concentrations is good (see Table 4). The simulations predict the correct increase in γ with molality. We have further

estimated the increase in γ for the 3.4 *m* concentration. Our simulation predicts a large increase of 8.1 mN/m. This result is well above the estimate obtained from the extrapolation of the linear regression obtained in the experiments. It would be very interesting to perform experiments to check the magnitude of the increase in γ for these high concentrations. These results will be useful both to test the simulation force fields and for CCS applications and analysis.

Table 4
The increase in the interfacial tension of the CO_2-H_2O interface as a function of salt concentration. $\Delta\gamma(m) = \gamma(m) - \gamma(0)$ is the difference between the interfacial tension at salt concentration m, $\gamma(m)$, and the interfacial tension without salt, γ(0) . [Exp.] and [Sim.] refer to "Experimental" (Ref. [25]) and "Simulation" (this work) results. See text for details.

Concentration/molal	$\Delta\gamma(m)[Exp.]/(mN/m)$	$\Delta\gamma(m)[Sim.]/(mN/m)$
1	1.43	1.6
2	2.86	2.8
3.4	-	8.1

3.2 Quartz-water-CO_2 contact angles at subcritical temperatures

Figure 4 shows a representative snapshot of the simulation set up used to estimate the contact angles θ. The simulations were performed using cells with dimensions (x,y,z) = (79, 103, 150) Å, and at constant temperature, 300 K and 350 K, in the canonical ensemble (N,V,T). A typical simulation consisted of 4608 SiO_2 groups, a droplet containing 1000 water molecules and a varying number of CO_2 molecules, between 0 and 4913, which was adjusted to simulate different CO_2 pressures (0-20 MPa). The SiO_2 slab was constructed using a pre-equilibrated crystal at 0.1 MPa pressure and replicated to fill the chosen area. The slab plane was located normal to the *z* axis. Periodic boundary conditions were employed in the three directions, x, y, and z. As indicated in the Methodology section, a soft wall was placed inside the simulation box to constraint the motion of the CO_2 and H_2O molecules to the upper plane of the simulation cell, i.e., $z>0$. Given the low vapour pressure of water at 300-350 K we did not observe a significant evaporation of molecules, only a few molecules would escape to the CO_2 phase (see e.g. Figure 4).

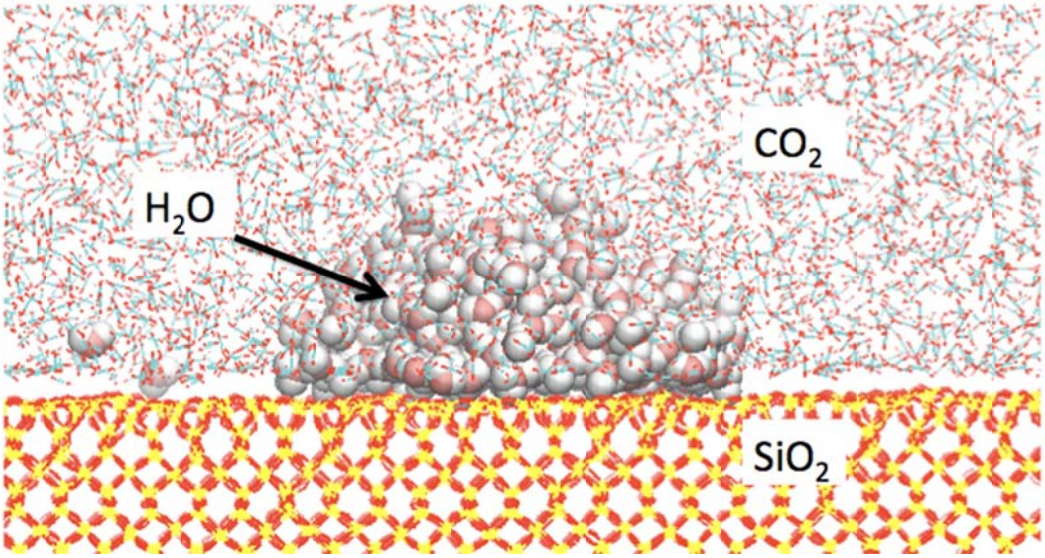

Figure 4. Snapshot of a representative configuration of an α-quartz-water-CO_2 system at 300 K and P(CO_2)=20 MPa, showing the simulation set up used to compute the contact angles. The quartz surface is perpendicular to the z axis.

The contact angles of water with the SiO_2 surface were obtained using a geometrical construction [60-62], which enabled us to fit the density contour of the water droplet to a circle. The density contour was obtained by calculating the density profile in cylindrical coordinates, using a cylinder of radius *r* and height *z* whose axis passes through the centre of mass of the water droplet; the centre of mass is normal to the SiO_2 surface. Figure 5 shows two examples of such density contours for two representative water droplets immersed in CO_2 in the vapour (left) and liquid (right) phases at 300 K. One iso-density line, 0.01 molecules/Å^3, was then fitted to a circle in order to estimate the contact angles.

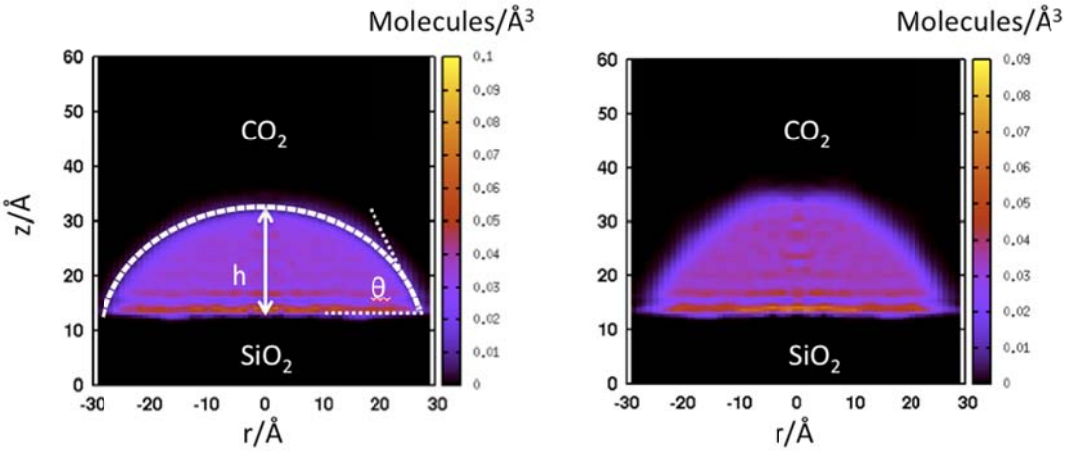

Figure 5. Density contours of two water droplets at two different CO_2 pressures and T = 300 K. Left: θ = 68^o ; P(CO_2)= 3.9 MPa. Right: θ = 79.5^o ; P(CO_2)= 18 MPa. θ was calculated using the equation: $\cos\theta = 1 - h/R$ [60-62]; where h is the maximum droplet height and R the radius of the circle (dashed line) as indicated in the left image.

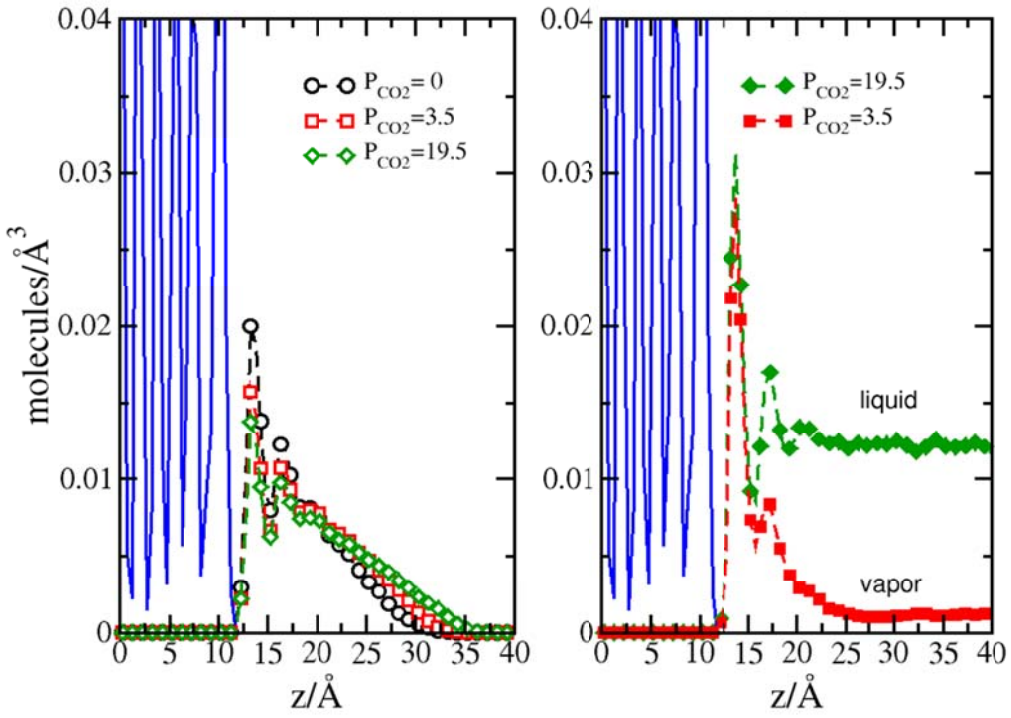

Figure 6. Density profiles normal to the quartz surface (profile from 0 to ~10 Å) at 300 K. Left panel, water density profile as a function of CO_2 pressure, 0, 3.5±0.2 MPa and 19.5±1.6 MPa. Right panel, CO_2 density profiles for vapour and liquid states.

The density contours displayed in Figure 5 show evidence for an enhanced density of water next to the quartz surface. The influence of the quartz surface on the water structure can also be quantified through the density profiles presented in Figure 6. These profiles show how the water layering is weakened by the presence of CO_2. Our simulations indicate that the Si-O-Si bridged α-quartz surface is hydrophilic as expected. In the absence of CO_2 , water spreads and wets the surface, compatible with a water-quartz contact angle of $\theta=0^o$. Other simulations of similar quartz surfaces at slightly higher temperatures, 318.15 K, have reported a partially wetting situation with relatively high contact angle values, 60^o [38]. In our case the formation of a wetting layer is compatible with the strong interaction of water with our quartz surface.

The main peak in the water density profile decreases with increasing CO_2 pressure (Figure 6, left panel), indicating a redistribution of water molecules in the water spherical cap (see Figure 5), which is connected to the increase in the water-quartz contact angle with pressure (see Figure 7). The CO_2 density profiles (see Figure 6-right panel) indicate that the CO_2 molecules interact strongly with the quartz surface investigated in this work. This strong interaction results in the formation of a physisorbed layer of CO_2 on the quartz surface at low pressures.

We have performed a systematic investigation of the water-quartz-CO_2 contact angles as a function of CO_2 pressure as this analysis is of particular relevance to CCS applications. Figure 7 displays a comparison of our results with data measured in

different experiments for quartz surfaces. Firstly, we note that the experimental results do not provide a unique answer with regard to the dependence of θ on CO_2 pressure. Both, experiments and simulations, agree on the hydrophilic character of the quartz surfaces, although the range of contact angles listed is rather large. Interestingly, the experiments of Bikkina [29] show a strong dependence of the contact angle values on the treatment of the surfaces. In that work large variations in the contact angles, up to 40^o, were reported. The differences between experimental data from different groups can also be significant, between 10^o and 20^o [27,29,32]. These data illustrate the difficulty in measuring the contact angles in the experiments. There are several factors that contribute to the experimental uncertainty in the measurements. The difficulty in keeping the surfaces clean is one of the most important ones. Also, the surfaces might feature different degrees of roughness, and can be chemically modified during the experiment, e.g., by changing the surface concentration of silanol groups on the quartz surface. In fact, in the experiments the quartz surface was effectively covered with silanol groups (note that silanol groups can further dissociate, point of zero charge of quartz is at pH = 3 [63]). In our simulations we have investigated a fully coordinated surface where the formation of silanol groups is not favoured. In addition only advancing or receding contact angles can be observed in the experiments, which leads to a possible range of θ [64]. In contrast, the simulations do not suffer from these uncertainties. The surface is well characterized, both, from a chemical and structural point of view, hence enabling a systematic investigation.

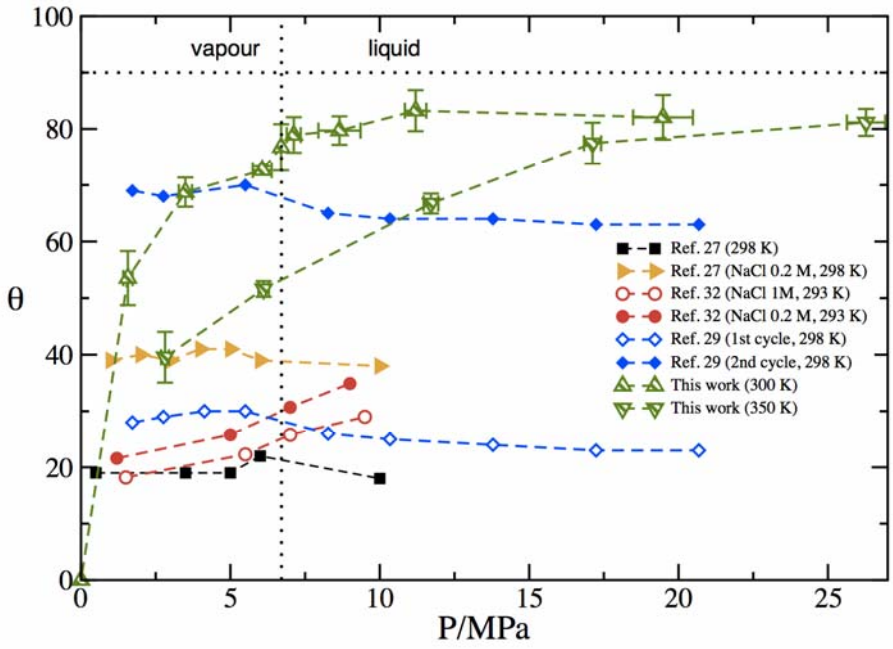

Figure 7. Contact angles of water with the quartz surface as a function of CO_2 pressure. Both simulation and experimental data are shown.

Our simulations indicate that in the whole pressure interval, the contact angle is < 90°. This result is compatible with the experiments, although the spread of experimental values is very large, hence precluding a quantitative comparison. We expect that the investigation of other surfaces, e.g., the under coordinated surface where water molecules dissociate forming silanol groups, would result in lower contact angles, as the water interaction with such a hydroxylated surface is significantly stronger [44].

Our simulations show that CO_2 has a major impact on the water contact angle (Figure 7). Addition of CO_2 inhibits wetting by water. For subcritical isotherms, T=300 K, the contact angle features a significant increase with CO_2 pressure, reaching a value of about 80° at the saturation pressure, 6.7 MPa, coincident with the formation of the CO_2 liquid phase. A further increase in pressure has a very minor effect on θ, which is essentially constant for a wide range of pressures (6-20 MPa). Following Young's equation, the contact angle results from a balance of interfacial tensions. For our case the contact angle is given by,

$$\cos\theta(P_{CO_2}) = \frac{\gamma_{CO_2-Q}(P_{CO_2}) - \gamma_{w-Q}}{\gamma_{CO_2-w}(P_{CO_2})}, \quad (8)$$

The applicability of Young's equation to investigate contact angles of nanoscale interfaces, such as the nanodroplets investigated in this work, has been validated in previous works [60-62]. To gain further insight on the relative strength of the quartz interactions with water and CO_2 we have estimated the difference between the interfacial tensions of the CO_2-quartz (γ_{CO_2-Q}) and water-quartz (γ_{w-Q}) interfaces (the numerator in equation (8)). We note that the water-quartz interfacial tension is a constant, i.e., independent of the CO_2 pressure. Using the contact angles reported in Figure 7 and the interfacial tensions in Figure 3, we estimate $\gamma_{CO_2-Q} - \gamma_{w-Q} \sim 5$ mN/m in the high-pressure region (P~20 MPa), consistent with a contact angle close to 90°. Figure 8 shows the variation of this interfacial tension difference as a function of CO_2 pressure. Our data show that both the CO_2-water and CO_2-quartz (again note that γ_{w-Q} is a constant) interfacial tensions feature a similar reduction in magnitude at pressures below the saturation one.

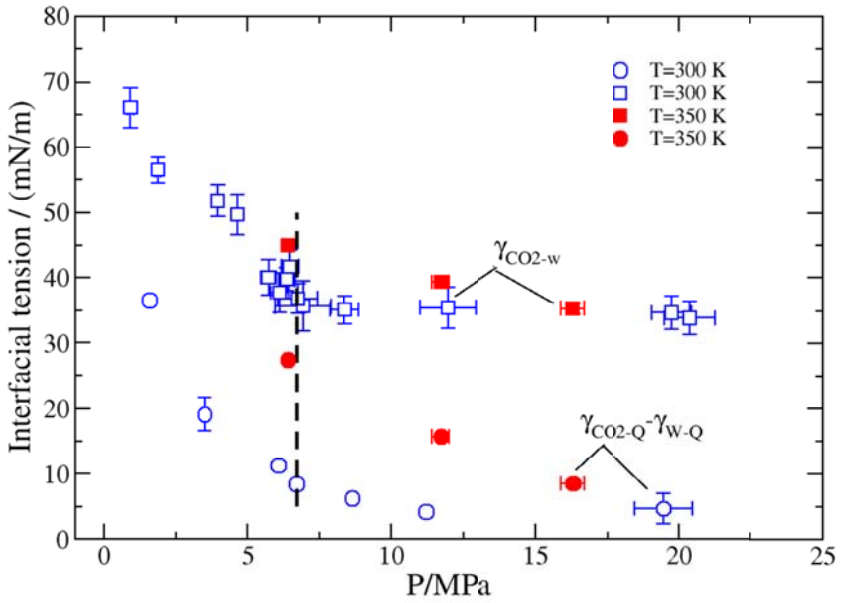

Figure 8. Interfacial tension difference between the CO_2-quartz and water-quartz interfacial tensions as a function of CO_2 pressure at T=300 K (open symbols) and 350 K (filled symbols). The vertical line corresponds to the CO_2 saturation pressure, 6.7 MPa. The error bars for $\gamma_{CO_2-Q} - \gamma_{w-Q}$, were obtained from an error analysis of the contact angles and water-CO_2 interfacial tensions.

Many of the experiments reported to date do not show a clear dependence of the contact angle on CO_2 pressure (see Figure 7). A notable exception are the experiments of Chiquet et. al. [32], who reported an increase in the measured contact angles with CO_2 pressure, hence following the same trends predicted by our simulations in the CO_2 vapour region. It is not possible to infer from these experiments the trends at higher pressures. Experiments conducted by a different author cover this important pressure range [29]. These experiments show that the contact angle is approximately independent of pressure for the whole pressure range (~2 to ~20 MPa). The constancy of θ as a function of pressure is consistent with our simulation results at high pressures, whereas these experiments and our MD simulations disagree on the dependency at lower pressures, particularly below the CO_2 saturation pressure.

3.3 Contact angles at reservoir temperatures

In order to study the effect of typical reservoir temperatures on the contact angle, θ, we performed additional simulations at 350 K (see Figure 7). We find that the temperature has a significant impact on the contact angles, with a reduction of ~20^o at low pressures (P~2.5 MPa). Interestingly, at higher pressures, which are more relevant to reservoir conditions, the impact on θ is minor. In fact the contact angles for 300 K and 350 K are identical within the statistical uncertainty of our computations for pressures above circa 17 MPa.

The reduction of θ with temperature must be the result of the interplay of the interfacial tension difference $\gamma_{CO_2-Q} - \gamma_{w-Q}$, with the water-$CO_2$ interfacial tension γ_{CO_2-w}. The experiments [23] and our simulations indicate that the increase in temperature results in an increase of γ_{CO_2-w}. If the difference $\gamma_{CO_2-Q} - \gamma_{w-Q}$ was constant, the contact angle would increase instead of decrease with temperature, which is what we observed in our simulations. It is clear then that the increase of temperature must modify the fluid-quartz interfacial tensions significantly. We can estimate the magnitude of the difference between these interfacial tensions, $\gamma_{CO_2-Q} - \gamma_{w-Q}$, by considering our simulation data for the interfacial tension (Table 3) and contact angles (Figure 7) at 350 K. We obtain $\gamma_{CO_2-Q} - \gamma_{w-Q}$=27.4 mN/m, 15.7 mN/m and 8.5 mN/m for P=6.4 MPa, 11.7 MPa and 16.3 MPa respectively. We find that $\gamma_{CO_2-Q} - \gamma_{w-Q}$ increases significantly with temperature at intermediate pressures, 5-15 MPa (see Figure 8), indicating a weakening of the CO_2-quartz interactions relative to the water-quartz ones. This weakening in the interactions drives the reduction in the contact angle observed at higher temperatures (350 K) and intermediate pressures.

For pressures relevant to CO_2 geo-sequestration, P~20 MPa, the fluid-quartz interactions as measured by $\gamma_{CO_2-Q} - \gamma_{w-Q}$ are similar both at 300 K and 350 K. Considering the temperature and pressure dependence of the contact angles, we conclude that, for the mineral surface investigated in this work, a moderate increase in temperature, ~50 K, would be beneficial for residual and structural trapping at low-moderate pressures (P~3-10 MPa), while such an increase in temperature would only have a minor positive impact at higher pressures, >17 MPa.

3.4 Brine-quartz-CO_2 contact angles as a function of salinity

We have analysed the impact of salt concentration on contact angles. To accomplish this analysis, we substituted some of the water molecules in the water droplet by NaCl ion pairs in order to generate two different salt concentrations: 1 and 4 m. These simulations were performed at 300 K.

As mentioned previously the impact of salt on θ is not well established. Some experiments indicate a decrease in θ upon addition of salt [32] whereas others report a significant increase [27]. We do not observe a systematic increase/decrease in the contact angles, the changes in the contact angles being close to the uncertainty of our computations. Our values are $66.5^o \pm 1.5^o$ for P=4.1±0.1 MPa and 1 molal NaCl concentration, and $70^o \pm 1.7^o$ for P=4.5±0.6 MPa and 4 molal NaCl concentration, as compared with ~69^o (interpolated from data given in Figure 7) under no salt conditions. The density contours and density profiles provide a route to visualize the ion distribution inside the water droplet, and the ions-quartz correlations. Figure 9 shows that the ions accumulate inside the droplet at both high (4 m) and low concentrations (1 m). This behaviour would be consistent with negative adsorption at the water-CO_2 interface. Indeed the addition of salt increases the interfacial tension of the water-CO_2 interface (see Table 4), hence following the Gibbs adsorption isotherm, a negative adsorption is expected. The density contours (see Figure 9) also suggests that the ions are not in direct contact with the surface. A more detailed analysis of the

density profiles, in this case the profile normal to the quartz surface, (see Figure 10), shows that the ions are separated from the quartz surface by one water layer. The density of this layer is fairly insensitive to the salt concentration. The ion distribution features a larger dependence on salt concentration though, with the ions undergoing a larger depletion from the quartz surface at high salt concentrations (cf. 1 m and 4 m cases in Figure 10).

In summary, our results show that the addition of salt has a minor effect both on the water interfacial structure, and on the water contact angles. These conclusions apply to low CO_2 pressures, ~4 MPa, which is a typical value investigated in the experiments (see Figure 7).

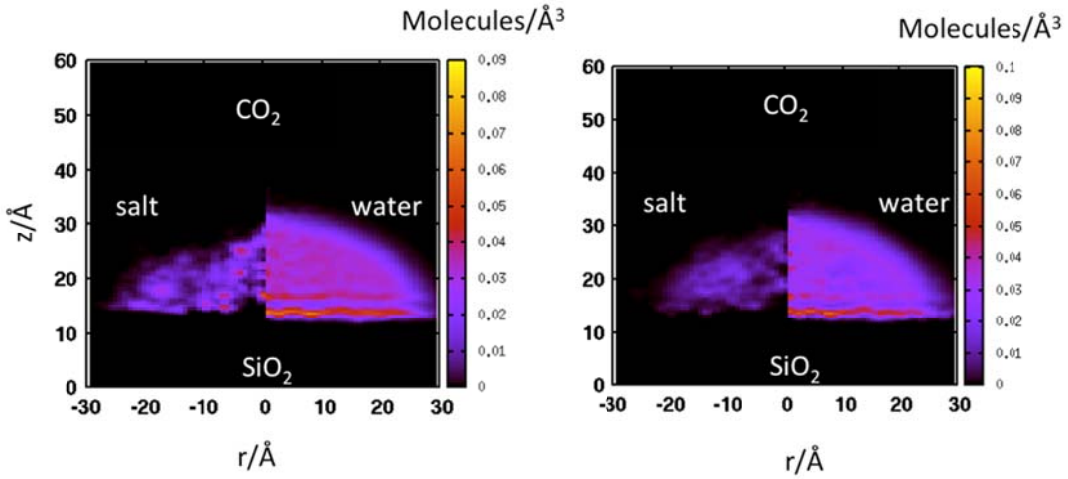

Figure 9. Density contours of two water droplets at P(CO_2)~4 MPa , T = 300 K, containing different amounts of NaCl. Left: 1 molal. Right: 4 molal. For each panel, the contour for r < 0, corresponds to NaCl, taken as an average of the Na^+ and Cl^- ion densities, and r >0, corresponds to water. The density of NaCl has been scaled by ×12 (1 molal) and ×2 (4 molal) to facilitate the comparison with the water densities.

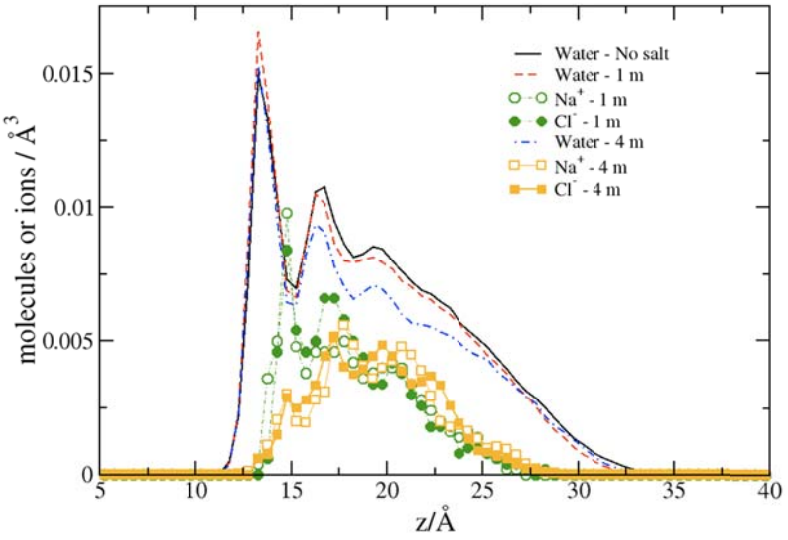

Figure 10. Density profiles of water and ions normal to the quartz surface at 300 K, P(CO_2)~4 MPa, and different NaCl concentrations. The densities of NaCl have been

scaled by ×20 (1 molal) and ×5 (4 molal) to facilitate the comparison with the water density.

4. Summary and Conclusions

We have developed a fully atomistic molecular dynamics model with which CO_2-brine interfacial tensions and CO_2-brine-quartz contact angles can be systematically investigated over a large range of thermo-physical conditions; our focus is on such conditions, which are most relevant to carbon geo-sequestration projects. Current experimental estimates of contact angles often involve very large uncertainties (Figure 7, [27,29-35]). Generally, uncertainties of such kind lead to low public acceptance of industrial CCS projects [65]; and consequently projects have been stopped, e.g. in Germany and the Netherlands. Hence there is a clear need to explore new approaches to access unequivocal information on interfacial properties such as contact angles. The simulation approach discussed in this paper provides a route to tackle this problem.

Our simulation model predicts a decrease in γ with increasing pressure; γ decreases until the CO_2 saturation pressure, P_{sat}, is reached. The simulation results show excellent agreement with the available experimental data for subcritical pressures [23-26]. However, the molecular dynamics simulations over predict γ for pressures > P_{sat} by circa 20%. Improving the agreement between the simulation and experiments in this pressure regime might require the introduction of non-additive corrections in the Lorentz-Berthelot combining rules. Preliminary calculations indicate that this is the case. Otherwise, the models capture two important features, namely the increase of interfacial tension with temperature at low and intermediate pressures 4-17 MPa, and the increase of interfacial tension with salt concentration in the range 1-3 m [23-26]. This clearly indicates that the negative ion adsorption is correctly predicted by the models.

In order to model the contact angles, we have considered a fully coordinated Si-O-Si bridged α-quartz surface in the CO_2-brine model. The surface is strongly water-wet as water completely spreads on this surface (without CO_2 present), indicative of a 0^o contact angle. The simulation model clearly shows the formation of a water monolayer in contact with the surface. The monolayer is not modified by addition of salt, but we find that CO_2 can displace water. In fact our simulations reveal a strong interaction between CO_2 and the quartz surface, which results in a strong modification of the contact angle upon increase of the CO_2 pressure. Hence, CO_2 inhibits wetting by water and results in a significant increase in θ. The contact angles follow the trends previously reported in a computer simulation investigation [35] and some experimental works [32].

Based on our computations we reach the following conclusions in terms of the contact angles:

a) at subcritical conditions, T=300 K, θ strongly increases with increasing pressure until approximately the saturation pressure of CO_2 is reached. This behaviour is mainly driven by the rapid change in the CO_2 density with pressure and the strong CO_2-quartz interaction. Above the saturation pressure,

θ increases slightly with further pressure increase. This is consistent with Chiquet et al.'s measurements [32].

b) θ decreases with temperature in the interval 0-17 MPa, consistent with experimental data [34]. Our analysis indicates that this reduction in the contact angle is driven by a significant weakening of the CO_2-quartz interaction relative to the water-quartz interaction. At higher pressures, ~20 MPa, the effect of temperature on the contact angle is shown to be minor,

c) Our simulations do not show evidence for a systematic increase or decrease of the contact angle with salt concentration (investigated for T = 300 K, P ≈ 4 MPa). The simulations indicate that the NaCl ions are depleted from the quartz surface, indicating there is a free energy barrier for ion adsorption. Hence, we expect they will not introduce large changes in the quartz-water interfacial free energy. It would be very interesting to analyse a different salt, which results in a large ion density enhancement at the interface. This will enable us to assess the dependence of the contact angles on salt composition.

d) In terms of structural and residual trapping, the MD results imply that lower pressures and higher temperatures are favourable storage conditions, while high salt concentrations can be tolerated as salinity has only a marginal influence. Other effects, such as decreased CO_2 density may however outweigh the benefits achieved with a lower θ.

Overall, our simulations demonstrate that the thermo-physical conditions can have a considerable impact on the water-CO_2-quartz contact angles and therefore structural and residual trapping capacities. The present simulation model may contribute to shed light on the large number of contrasting experimental measurements of contact angles and enable the microscopic investigation of the interfacial properties of aqueous solutions with mineral surfaces, which are difficult to perform given the intrinsic experimental difficulties associated with contact angle measurements.

Acknowledgement

The authors would like to thank the Imperial College High Performance Computing Service for providing computational resources. Financial support for this work was provided by the Royal Society. FB would like to thanks the EPSRC for the award of a Leadership Fellowship.

References

[1] X. Gao, L. Jiang, Nature 432 (2004) 36.

[2] A.R. Hutchinson, S. Iglauer, Int J Adhes Adhes 26 (2006) 555.

[3] Y.-J. Liu, N.M. Navasero, H.-Z. Yu, Langmuir 20 (2004) 4039.

[4] B. Metz, O. Davidson, H. de Coninck, M. Loos, L. Meyer (Eds.), Intergovernmental Panel on Climate Change Special Report on Carbon Dioxide Capture and Storage, Cambridge University Press, 2005.

[5] M.A. Hesse, F.M., Orr, H.A., Tchelepi, J. Fluid Mech 611 (2008) 35.

[6] R. Juanes, E.J. Spiteri, F.M. Orr, M.J. Blunt, Water Resour. Res. 42 (2006) W12418.

[7] S. Iglauer, A. Paluszny, C.H. Pentland, M.J. Blunt, Geophys. Res. Lett. 38 (2011) L21403.

[8] C.H. Pentland, R. El-Maghraby, S. Iglauer, M.J. Blunt, Geophys. Res. Lett. 38 (2011) L06401.

[9] S. Iglauer, in: H. Nakajima (Ed.), Mass Transfer, InTech, Rijeka, 2011, 233.

[10] A. Riaz, M.A. Hesse, H.A. Tchelepi, F.M. Orr, J Fluid Mech 548 (2006) 87.

[11] I. Gaus, Int. J. Greenh. Gas Con. 4 (2010) 73.

[12] M. Naylor, M. Wilkinson, R.S. Hazeldine, Mar. Petrol. Geol. 28 (2011) 1083.

[13] R. Qi, T.C. LaForce, M.J. Blunt, Int. J. Greenh. Gas Con. 3 (2009) 195.

[14] E. J. Spiteri, R. Juanes, M.J. Blunt, F.M. Orr, SPE J. 13 (2008) 277.

[15] L.W. Lake, Enhanced Oil Recovery, SPE Publications: Richardson, 1984.

[16] S. Iglauer, M. Fernø, P. Shearing, M.J. Blunt, J. Colloid Interf. Sci. 375 (2012) 187.

[17] S.K. Al-Mansoori, E. Itsekiri, S. Iglauer, C.H. Pentland, B. Bijeljic, M.J. Blunt, Int. J. Greenh. Gas Con. 4 (2010) 283.

[18] S.K. Al-Mansoori, S. Iglauer, C.H. Pentland, M.J. Blunt, Adv. Water Resour. 32 (2009) 1535.

[19] C.H. Pentland, Y. Tanino, S. Iglauer, M.J. Blunt, SPE 133798, SPE An. Tech. Con. Proc. (2010).

[20] P. Gittins, S. Iglauer, C.H. Pentland, S.K. Al-Mansoori, S. Al-Sayari, B. Bijeljic, M.J. Blunt, J. Porous Media 13 (2010) 591.

[21] S. Iglauer, S. Favretto, G. Spinelli, G. Schena, M.J. Blunt, Phys. Rev. E 82 (2010) 056315.

[22] S. Iglauer, W. Wülling, C.H. Pentland, S.K. Al-Mansoori, M.J. Blunt, SPE J. 16 (2011) 778.

[23] A. Georgiadis, G. Maitland, J.P.M. Trusler, A. Bismarck, J. Chem. Eng. Data 55 (2010) 4168.

[24] A. Hebach, A. Oberhof, N. Dahmen, A. Kogel, H. Ederer, E. Dinjus, J. Chem. Eng Data 47 (2002) 1540.

[25] C. Chalbaud, M. Robin, J.M. Lombard, F. Martin, P. Egermann, H. Bertin, Adv. Water Resour. 32 (2009) 98.

[26] B.-S. Chun, G.T. Wilkinson, Ind. Eng. Chem. Res. 34 (1995) 4371.

[27] D.N. Espinoza, J.C. Santamarina, Water Resour. Res. 46 (2010) W0753.

[28] B. Kvamme, T. Kuznetsova, A. Hebach, A. Oberhof, E. Lunde, Comp. Mater. Sci. 38 (2007) 506.

[29] P.K. Bikkina, Int. J. Greenh. Gas Con. 5 (2011) 1259.

[30] J. Mahadevan, Int. J. Greenh. Gas Con. 5 (2012) in press.

[31] P.K. Bikkina, Int. J. Greenh. Gas Con. 5 (2012) in press.

[32] P. Chiquet, D. Broseta, S. Thibeau, Geofluids 7 (2007) 112.

[33] J.L. Dickson, G. Gupta, T.S. Horozov, B.P. Binks, K.P. Johnston, Langmuir 22 (2006) 2161.

[34] D. Yang, Y. Gu, P. Tontiwachwuthikul, Energy Fuels 22 (2008) 504.

[35] J. Mills, M. Riazi, M. Sohrabi, SCA2011-6, Proc. Int. Symp. Soc. Core Ana. (2011).

[36] D. Broseta, private communication (2010).

[37] W.J. Plug, J. Bruining, Adv. Water Resour. 30 (2007) 2339.

[38] S.-Y. Liu, X.-N. Yang, Y. Qin, Chinese Sci. Bull. 55 (2010) 2252.

[39] J.L.F. Abascal, C. Vega, J. Chem. Phys. 123 (2005) 234505.

[40] J.G. Harris, K.H. Yung, J. Phys. Chem. 99 (1995) 12021.

[41] C. Vega, E. de Miguel, J. Chem. Phys. 126 (2007) 154707.

[42] L.C. Nielsen, I.C. Bourg, G. Sposito, Geochim. Cosmoschim. Ac. 81 (2012) 28.

[43] F. Biscay, A. Ghoufi, V. Lachet, P. Malfreyt, J. Phys. Chem. B, 113 (2009) 14277.

[44] Z. Du, N.H. de Leeuw, Surf.Sci. 554 (2004) 193.

[45] W.A. Adeagbo, N.L. Doltsinis, K. Klevakina, J. Renner, ChemphysChem 9 (2008) 994.

[46] B.W.H. van Beest, G.J. Kramer, R.A. van Santen, Phys. Rev Lett. 64 (1990) 1955.

[47] J. Alejandre, G.A. Chapela, F. Bresme, J.P. Hansen, J. Chem. Phys. 130 (2009) 174505.

[48] P.P. Ewald, Ann. Phys., Leipzig, 64, (1921) 253.

[49] DL_POLY is a package of molecular simulation routines written by W. Smith and T.R. Forester, copyright The Council for the Central Laboratory of the Research Councils, Daresbury Laboratory at Daresbury, Nr. Warrington (1996).

[50] M. Gonzalez-Melchor, F. Bresme, J. Alejandre, J. Chem. Phys. 122 (2005) 104710.; M. Gonzalez-Melchor, P. Orea, J. Lopez-Lemus, F. Bresme and J. Alejandre, J. Chem. Phys. 122 (2005) 094503

[51] S.R.P. da Rocha, K.P. Johnston, R.E. Westacott, P.J. Rossky, J. Phys. Chem. *B*, 105 (2001) 12092.

[52] H.T. Schaeff, B.P. McGrail, Proc. 7th Int. Con. Greenh. Gas Con. Tech. *(2004).*

[53] T.L. Tarbuck, G.L. Richmond, J. Am. Chem. Soc. 128 (2006) 3256.

[54] B. Kvamme, T. Kuznetsova, A. Hebach, A. Oberhof, E. Lunde, Comp. Mater. Sci. 38 (2007) 506.

[55] L. Zhao, S. Lin, J.D. Mendenhall, P.K. Yuet, D. Blankschtein, J. Phys. Chem. B 115 (2011) 6076.

[56] H. Zhang, S.J. Singer, J. Phys. Chem. A 115 (2011) 6285.

[57] NIST Chemistry Webbook.

[58] A. Wynveen, F. Bresme, J. Chem. Phys. 124 (2006) 104502.

[59] X. Xie, Z. Fan, X. Liu, Y. Lu. J. Geochem. Explor. 89 (2006) 432.

[60] F. Bresme, N. Quirke, Phys. Rev. Lett., 80 (1998) 3791.

[61] F. Bresme, N. Quirke, J. Chem. Phys. 112 (2000) 5985.

[62] F. Bresme, M. Oettel, J. Phys. Condens. Matter, 19, (2007) 413101.

[63] K. Bourikas, J. Vakros, C. Kordulis, A. Lycourghiotis, J. Phys. Chem. B 107 (2003) 9441.

[64] H.-J. Butt, K. Graf, M. Kappl, Physics and Chemistry of Interfaces, Wiley-VCH, Weinheim, 2006.

[65] B.W. Terwel, E. ter Mors, D.D.L. Daamen, Int. J. Greenh. Gas Con. 9 (2012) 41.